applied sciences

MDPI

Article

Personalised High Tibial Osteotomy Surgery Is Accurate: An Assessment Using 3D Distance Mapping

Andrea Varaschin [1], Harinderjit Singh Gill [2], Stefano Zaffagnini [3], Alberto Leardini [1], Maurizio Ortolani [1], Fabio Norvillo [4], Alisdair MacLeod [2], Giacomo Dal Fabbro [3], Giorgio Cassiolas [1], Alberto Grassi [3] and Claudio Belvedere [1,*]

[1] Movement Analysis Laboratory, IRCCS Istituto Ortopedico Rizzoli, 40136 Bologna, Italy; andrea.varaschin@ior.it (A.V.); leardini@ior.it (A.L.); maurizio.ortolani@ior.it (M.O.); giorgiocassiolas.lavoro@gmail.com (G.C.)
[2] Centre for Therapeutic Innovation/CBio, Department of Mechanical Engineering, University of Bath, Bath BA2 7AY, UK; rg433@bath.ac.uk (H.S.G.); a.macleod@bath.ac.uk (A.M.)
[3] II Clinic of Orthopaedics and Traumatology, IRCCS Istituto Ortopedico Rizzoli, 40136 Bologna, Italy; stefano.zaffagnini@unibo.it (S.Z.); giacomo.dalfabbro@studio.unibo.it (G.D.F.); alberto.grassi@ior.it (A.G.)
[4] Diagnostic and Interventional Radiology, IRCCS Istituto Ortopedico Rizzoli, 40136 Bologna, Italy; fabio.norvillo@ior.it
* Correspondence: belvedere@ior.it

Abstract: Early-stage knee osteoarthritis is often suitable for treatment with high tibial osteotomy (HTO). This is an effective joint-preserving treatment, resulting in good postoperative outcomes. To overcome the limitations of traditional HTO, the surgical technique and correction accuracy can be enhanced by personalised procedures using three-dimensional digital planning and metal additive manufacturing, The purpose of this clinical trial study was to evaluate the three-dimensional accuracy of a new personalised HTO procedure, using modern imaging techniques, 3D modelling, and distance map analysis (DMA). Twenty-five patients were treated with the personalised HTO procedure. Before surgery and after 6 months, they underwent clinical evaluation scoring, radiographic imaging, and computed-tomography scanning to generate morphological models. Specifically, preoperative tibia models were used to plan the tibia correction and the design and position of the fixation plate. Preoperative, planned, and postoperative models were imported in computer-aided and designing software (Geomagic ControlTM 2014, 3D Systems, Rock Hill, SC, USA) for DMA implementation to assess geometrical differences between model surfaces. A very good reproduction of the planned tibia morphology was achieved postoperatively (average differences between −0.9 mm and 1.4 mm). DMA values associated with fixation-plate deformation were less than 1 mm, similar to those for plate-to-tibia surface-contour matching. Overall, personalised digitally planned HTO utilising three-dimensional printed surgical guides and plates enables accurate planned correction and plate placement.

Keywords: high tibial osteotomy; personalised orthopaedic treatment; 3D printing; distance map analysis; computational modelling; computational planning

Citation: Varaschin, A.; Gill, H.S.; Zaffagnini, S.; Leardini, A.; Ortolani, M.; Norvillo, F.; MacLeod, A.; Dal Fabbro, G.; Cassiolas, G.; Grassi, A.; et al. Personalised High Tibial Osteotomy Surgery Is Accurate: An Assessment Using 3D Distance Mapping. *Appl. Sci.* **2024**, *14*, 9033. https://doi.org/10.3390/app14199033

Academic Editor: Gusztáv Fekete

Received: 26 July 2024
Revised: 24 September 2024
Accepted: 25 September 2024
Published: 6 October 2024

1. Introduction

Osteoarthritis (OA) of the knee carries a huge personal [1] and societal burden [2,3]. The global prevalence of knee OA is high, being highest in Asia (19.2%), followed by North America (15.8%) and Europe (13.4%) [4]. Incidence of knee OA is strongly associated with increasing age [5]. As the global population ages, the prevalence of the disease is expected to increase [6] and to have a significant impact on healthcare systems for the coming decades [7]. In addition, previous predictions of OA prevalence have underestimated actual increase in the burden of this disease [8], and the increase in prevalence is greater than explained by ageing and increased BMI [9]. Knee OA is associated also with increased

cardiovascular disease and mental health conditions [10], as well as greater than a 15% increase in premature all-cause mortality [11].

Joint replacement is considered as the gold standard in treating knee OA. The demand for this treatment is growing and projected to at least double from 2015 levels by 2030 [12], with studies even predicting far higher demand [13]. However, joint replacement is only applicable for end-stage disease [14], and the majority of OA patients fall into the treatment gap, possibly for decades [15]. Nonsteroidal anti-inflammatory drugs and opioids are the most prescribed pain management medications for OA [16]; however, this form of treatment is associated with poor clinical outcomes, increased mortality, and healthcare resource utilisation [17]. It is worrying that the prevalence of opioid prescription has increased, as a 44% prevalence of patients prescribed opioids while waiting for knee replacement has been recently reported [18].

The majority of knee OA begins in the medial compartment [19] and it is often suitable for treatment with unicompartmental knee replacement (UKR) or high tibial osteotomy (HTO), which have broadly similar indications [20]; however, it is recommended that HTO is used at earlier stages of OA [21]. The consequences of medial knee OA is that the affected knee bows out laterally, which is termed varus knee alignment. HTO surgery aims to correct this alignment closer to neutral. The alignment of the knee is clinically measured by the angle between the mechanical axis of the femur and that of the tibia in the frontal plane, termed the hip–knee–ankle (HKA) angle. The convention used in this work is that HKA $> 180^{\circ}$ is varus alignment. Patient outcomes are generally reported to be similar between UKR and HTO, with larger range of motion and more activity observed after HTO [21–23]. Recently a number of studies have shown a relatively high early failure rate for UKR. Based on data from the United Kingdom National Joint Registry, UKR revision rates are 2.5 times higher than those from total knee replacement for UKR surgeries performed by the highest quartile volume surgeons, and even 3.9 times higher for those performed by the lowest quartile [24]. This concurs with a previous report based on United States data [25], and also with another report based on the Italian regional registry data [26]. The 2021 United Kingdom National Joint Registry report shows that UKR revision rates are approximately 15% for males and 16% for females at ten years after surgery, rising to 22% for males and 24% for females at 15 years [27].

There is a clear need for effective joint-preserving treatments that can be utilised at a relatively early stage of knee OA. HTO has a well-established clinical track record and is suitable for relatively young patients. However, HTO surgery is perceived as technically challenging, and surgeons are concerned about achieving their planned correction [28]. Achieving the planned correction is difficult, and the clinical outcome is apparently highly dependent upon this [29,30]. This perception may be the major reason for a decline in HTO surgery in the last two decades [20].

With the coming together of advances in three-dimensional (3D) digital planning and metal additive manufacturing, personalised, or patient specific, HTO has now become a practical reality [31,32]. Based on these technologies, personalised surgical procedures offer the potential for simplified surgical techniques and increased correction accuracy. In silico trials have demonstrated the safety of 3D-printed personalised HTO, comparable to generic off-the-shelf devices [33], and excellent functional recovery was observed in a preliminary clinical trial [34] on patients treated using a novel fully personalised HTO procedure [32]. This technique uses 3D morphological reconstructions of the patient's knee anatomy from medical imaging to perform customised planning. The final surgical plan generates the design of the surgical instrumentation, i.e., the surgical guide for the osteotomy, and of the fixation plate. The surgical guide and plate are manufactured by 3D printing in medical-grade titanium alloy (Ti6AL4V) powder. This new surgical procedure overcomes the limitations of traditional HTO techniques, which use generic off-the-shelf plates and can have lower correction accuracy with a negative impact on patient outcomes [31,35]. To date, the accuracy of this new personalised HTO overall procedure has been evaluated in the preclinical phase and a first-in-human clinical trial,

showing better performance than that reported for conventional techniques, especially in terms of postoperative achievement of the preoperative surgical planning [36,37]. The most used clinical measure of accuracy is the hip–knee–ankle (HKA) angle measured from long-leg radiographs, comparing the achieved change in HKA to the planned change in HKA. The HKA angle change is achieved by changing the orientation of the tibial plateau with the surgical osteotomy. In the personalised procedure, a 3D geometric model is created from the surgical planning process, giving the planned tibial correction and the planned location of the plate. By analysing patient-specific 3D models reconstructed from computed tomography (CT) imaging performed PREoperatively (PRE) and POSToperatively (POST), and the 3D models resulting from the surgical PLAnning process (PLA), the effects of the surgery and the accuracy of achieving the planned osteotomy and plate location can be quantified by distribution of distances between the surfaces of appropriately selected reference and test models. Distance map analysis (DMA), which has been previously utilised in similar contexts [38,39], can offer a valuable support to these evaluations. Of note, image analysis and segmentation techniques, the related reconstruction of 3D bone geometry, and the identification of anatomical landmarks require special attention and must be approached with care, as much of the accuracy in data processing depends primarily on them [40,41].

The purpose of the present study was to evaluate the overall 3D accuracy of this new surgical procedure for personalised HTO, using modern imaging techniques, 3D modelling, and DMA. The present analysis is part of the first-in-human clinical trial for this procedure.

2. Materials and Methods

The investigation workflow, along with information on the patients enrolled and the overall study design, are presented below. Details are provided on the instruments used and data analyses performed, as well as the technical solutions adopted to best achieve the purpose of the present study.

2.1. Study Design

The present study concerns further investigations related to a first-in-human clinical trial using a novel procedure for personalised HTO [32,37]. This clinical trial received institutional review board approval (Ethics Committee of the Area Vasta Emilia Centro-CE AVEC, code: 623/2019/Disp/IOR, Italy) and governmental regulatory approval (Italian Ministry of Health. Directorate General of Medical Devices and Pharmaceutical Services, DGDMF.6/P/I.5.i.m.2/2019/1351), and all patients provided informed consent. This was a single-arm prospective interventional trial, registered at ClinicalTrials.gov (NCT04574570).

2.2. Patient Cohort

The study inclusion/exclusion criteria and relevant power-analyses of the determination of the patient population, as well as the demographic and clinical data of the clinical trial, have previously been published in detail by these authors [34,37] and reported briefly as follows.

Relevant inclusion/exclusion study criteria are summarised here below:

- Inclusion: age 40–65 years; BMI < 40; varus deformity <20°; diagnosis of non-inflammatory degenerative joint disease; mono-compartmental medial knee OA.
- Exclusion: BMI $\geq$ 40; patients' inability to provide informed consent; patients' non-compliance with postoperative rehabilitation and evaluation schedules; patients with comorbidities or with very poor bone quality; other lower limb joint surgeries.

A cohort of 25 patients was selected and treated for personalised HTO: females/males: 6/19; age (mean $\pm$ standard deviation): 54.4 $\pm$ 7.4 years (min to max: 39 to 65 years); Body Mass Index: 26.8 $\pm$ 4.0 (20.9 to 37.5); Kellgren–Lawrence grade: 2.6 $\pm$ 0.5 (2 to 3); PRE hip–knee–ankle (HKA) angle: 189.3° $\pm$ 3.2° (184.0° to 195.7°; HKA > 180 indicates varus knee alignment).

As this was an initial single-arm trial in humans using the novel personalised HTO procedure, a power study was not necessary. Among the various evaluations within the clinical trial [31,34,42], all patients underwent comprehensive medical imaging inspections (see next section) and clinical examination PRE and six months POST operation. Clinical outcomes were based on patient-reported outcome measures, including the Knee Osteoarthritis Outcome Score (KOOS) [43], here considered as a total score averaged across all domains and also as individual domains (0 = worst condition, 100 = best condition), and the visual analogue score (VAS) for pain during activity [44] (VAS pain score, 0 = no pain, 10 = worst pain).

2.3. Imaging, Surgical Planning and Procedure

Within a four-month window prior to surgery (condition PRE), each patient underwent medical imaging to enable digital surgical planning. This included frontal bi-pedal standing long-leg radiographs, and weight-bearing CT (WBCT) scans of the affected knee in single leg upright stance using a cone-beam CT scanner (OnSight 3D Extremity, Carestream, Rochester, NY, USA). This imaging device uses a rotating X-ray source with three emitters, capturing accurate images with a wide field of view and allowing a volumetric acquisition with a single source rotation (current and energy: 5 mA and 80 kVp; dose: 0.024 mSv; rotation and exposure time: 25 s and 21 s; scan rotation angle: 216°; field-of-view: 216 × 216 mm; pixel pitch: 0.13 mm; matrix: 884 × 884; scanning slice thickness: 0.26 mm; voxel size: 0.26 isotropic) [45], with an extremely low radiation dose [46,47]. Relevant CT scan images were then segmented (Mimics Innovation Suite version 22.0, Materialise, Leuven, Belgium) to generate a 3D geometrical model of the intact (i.e., PRE or before the osteotomy surgery) proximal tibial bone surface in STereo-Lithography-interface (STL) format. To generate each 3D bone model, semi-automatic density-based segmentation was used, with cortical bone density set at 400 ± 100 HU. The segmented mesh was processed to remove holes resulting in a closed surface mesh. This process relied on three sequential steps: (a) selection of the outer faces by a linked surface faces approach; (b) surface reconstruction using a screened Poisson approach; (c) isotropic re-meshing with a target triangle edge length of 0.8 mm.

The PRE model for the tibial bone was subsequently used in the surgical planning stage (i.e., PLA) for the personalised HTO. Note that in the generation of the PLA model, the segmentation software can apply additional iterations of smoothing and decimation of the mesh according to predefined parameters for 'high' export quality to have an optimal reference bone surface in surgical planning. This stage included the definition of the virtual position and orientation of the proximal tibia osteotomy (Figure 1), including position and inclination of the associated fixation screws, as well as the simulation of the amount of wedge opening about the hinge [33,36].

Using appropriate software for computer-aided modelling and designing (Rhinoceros, Rhino 7 version, Robert McNeel & Associates, Seattle, WA, USA; Geomagic Freeform, 3D Systems, Rock Hill, SC, USA), the PLA geometrical models of the virtual proximal tibial surface after wedge opening and of the corresponding custom surgical guide, as well as of the personalised plate to fix the osteotomy, were designed and generated in STL file format. These PLA models of the guide and plate were then 3D printed (TOKA Personalised HTO, Orthoscape, 3D Metal Printing Ltd., Bath, UK; 3D printer: AM250, Renishaw plc, Wotton-under-Edge, UK) in medical-grade titanium alloy (Ti6AL4V, ASTM F136 grade 23), delivered to the hospital, and made available for the surgery after steam sterilization [32].

All surgeries were performed by a single surgeon. In addition to the surgical steps of a standard HTO, the present personalised procedure [32] included the fixation of the patient-specific surgical guide to perform the bone osteotomy, the drilling of bone holes to accommodate the screws for the fixation plate, and also the osteotomy opening mechanism, all according to the preoperative planning. During surgery, once the plate was fixed, the resulting wedge-shaped opening of the proximal tibia was filled with bone allograft from the institutional bone bank, followed by the final suture.

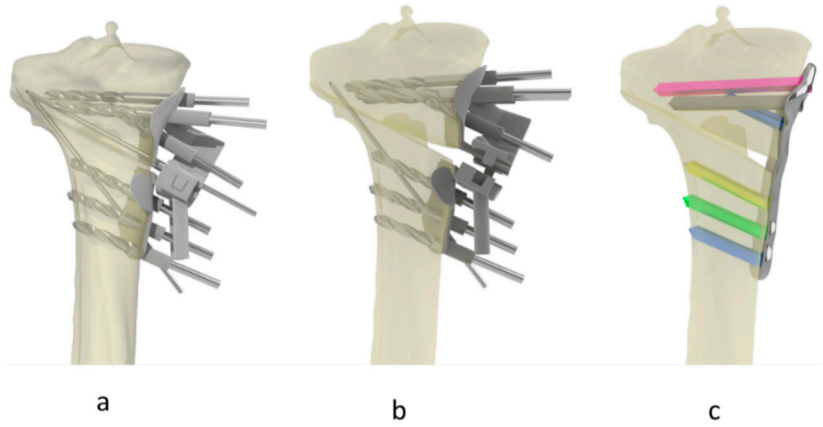

Figure 1. Planning on CT scan-derived geometry allows placement of tibial cuts and design of personalised jig and plate. (**a**) Tibial cuts with surgical jig in closed position. (**b**) Surgical jig opened to required correction. (**c**) Osteotomy stabilised with personalised plate (NB planning also gives the appropriate screw length to use, screw lengths are indicated by color).

After surgery, returning to full normal activity was recommended by following a standard rehabilitation program. Postoperatively at six months follow-up, the same preoperative imaging procedure was repeated. The corresponding WBCT scans were used to generate 3D geometric models (i.e., POST) of the proximal tibial bone surface after surgery, including the opening wedge, and of the osteotomy fixation plate in its actual positioning. Metal ands are possible when CT scanning patients who have metal devices implanted; the Carestream system's built-in metal artefact reduction software [48] was used to process the scans prior to segmentation for generating the POST 3D models.

2.4. Distance Map Analysis

The STL models generated in the three PRE, PLA, and POST stages were imported in computer-aided modelling and designing software (Geomagic, 3D Systems, Rock Hill, SC, USA) to implement DMA for the assessment of geometrical differences between pairs of selected model surfaces (Figure 2).

DMA allows quantifying the shortest distance between the mesh points of two selected surfaces facing each other, one surface being called "Test" and the other "Reference". A 3D colour-coded map of distances was then generated and displayed on the Reference object, with each colour associated with a different surface-to-surface distance interval. For this, Geomagic's "3D Comparison" tool was used, the relevant parameters of which were set to calculate and to export a number of DMA-related values. To identify the minimum distances between surfaces, the parameters "critical angle" and "maximum deviation" were set to 180° and 10 to 20 mm, respectively; the former was set to allow recognition of the maximum deviation, while the latter was adjusted according to the specific comparison and the expected maximum values. By definition, differences shown by DMA on the Reference surface were marked as positive (represented by progressive yellow/red areas) or negative (represented by progressive light blue/dark areas) if the Test surfaces were outside (i.e., separation) or inside (i.e., penetration) the Reference surfaces, respectively. DMA output consisted of the following values: Positive Maximum Distance (PMD) and Negative Maximum Distance (NMD), Positive mean Distance ($\overline{PD}$) and Negative mean Distance ($\overline{ND}$), and DMA standard deviation (DSD). The two mean distances, together with the DSD, are the most useful in determining deviations between two surfaces, and these were the focus of the analysis (Appendix A provides all DMA outputs for completeness).

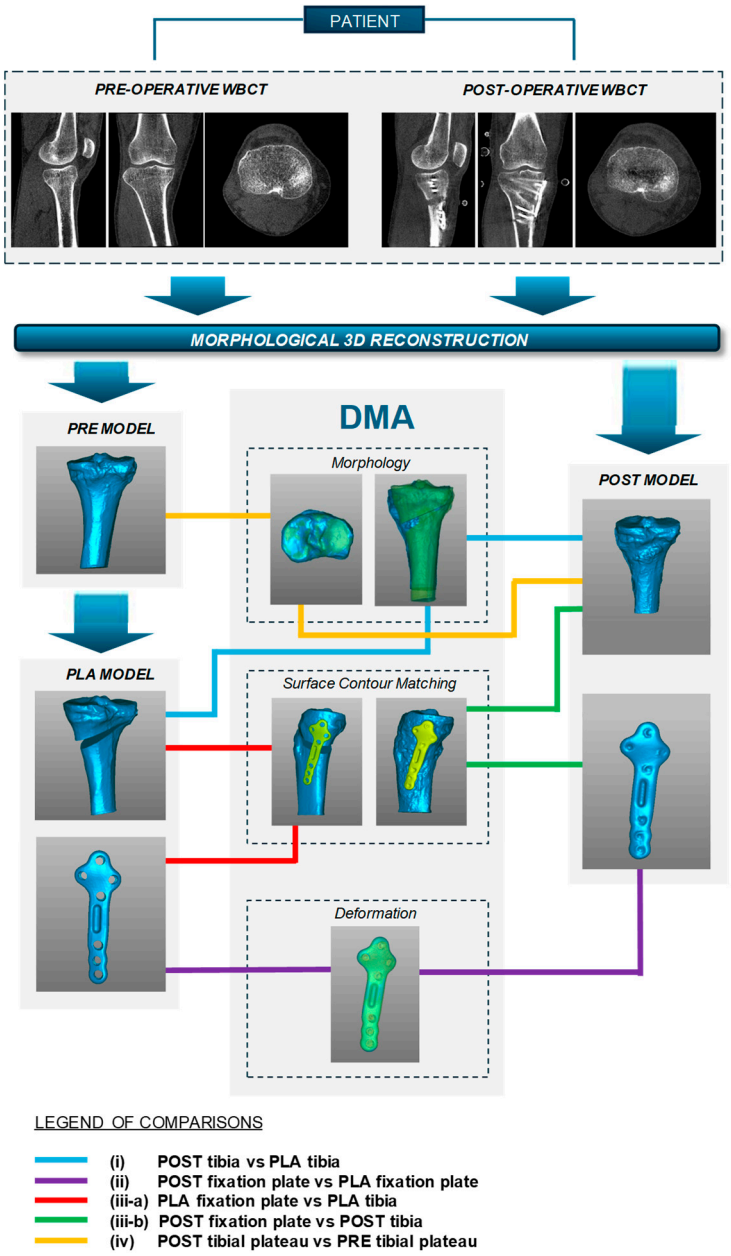

Figure 2. Diagram of the DMA workflow.

The following surface-to-surface comparisons were performed via DMA, with relevant "Reference" and "Test" surfaces being reported in brackets:

(i) POST tibia ("Test") versus PLA tibia ("Reference"), to check whether the planned new proximal tibial alignment had been achieved surgically;

(ii) POST fixation plate ("Test") versus PLA fixation plate ("Reference"), to check possible fixation-plate deformation after surgery with respect to the reference planned design;

(iii-a) PLA fixation plate ("Test") versus PLA tibia ("Reference"), to check planned plate-to-bone surface contour matching;

(iii-b) POST fixation plate ("Test") versus POST tibia ("Reference"), to check the achieved plate-to-bone surface contour matching;

(iv) POST tibial plateau ("Test") versus PRE tibial plateau ("Reference"), to check for changes in the plateau surface only (e.g., due to OA progression), independently from the correction performed with HTO.

Of note, prior to the implementation of DMA, best-fit model registration based on the Iterative Closest Point (ICP) algorithm in Geomagic was performed considering the tibial

diaphysis in comparison step i, i.e., the only tibial position which remains identical among the comparisons, or the overall morphologies in all other cases.

2.5. Data Processing

Clinical and radiological evaluations are reported in terms of mean ± standard deviation. A repeated measures ANOVA was performed to compare the effect of follow-up time on each patient-reported outcome measure after verifying normal distribution, as reported elsewhere by these authors [37] and summarised here in Section 3.

The mesh density data and the DMA outputs were not normally distributed (Kolmogorov–Smirnov). Hence, these values are reported in terms of median values, in addition to mean ± standard deviation. Consequently, the Mann–Whitney–Wilcoxon test was utilised for data comparison on mesh density data between PRE, PLA, and POST conditions.

For DMA outputs, differences between surfaces up to ±1 mm were considered acceptable. This threshold was inferred by considering the slicing resolution of the present WBCT and validation values of DMA on calibration reference objects previously reported by these authors [37].

In addition to standard DMA outputs and considering the above-mentioned deviation threshold, for each patient, further evaluations were executed starting from tables exported from Geomagic reporting the DMA values associated to each point of the Reference surface. From these, the percentage of points with DMA values within three following DMA intervals (Δ) in millimetres was calculated: (a) $-1 \leq \Delta \leq 1$, (b) $\Delta < -1$, and (c) $\Delta > 1$. The first interval, namely, the safety zone, indicates no or limited surface-to-surface deviations, while the second and third intervals indicate separation or penetration, respectively. Mean ± standard deviation over all analysed patients were also calculated for these percentage values.

In all comparisons, a p-value of less than 0.05 was taken to reveal statistically significant differences; otherwise, non-significance (NS) was indicated.

Data processing was performed using Matlab (Matlab®, R2022a The MathWorks, Inc., Natick, MA, USA).

3. Results

The findings are presented below, firstly of the clinical outcomes and measurement of overall leg alignment from pre- and postoperative radiographs, and then of the outcome of distance map analyses. The first part of the results confirms excellent outcomes through standard assessment methods and are supportive of the good DMA results. This section consists of tables (additional variables are reported in Appendix A), and boxplots related to the DMA parameters analysed, as well as figures showing morphologic discrepancies between PRE, PLA, and POST models for both bone and fixation plate. In detail, analysis of the distance maps was performed for all patients in the cohort, but the figures below refer to one representative patient; for completeness, screenshots of the DMA software for an alternative patient case are also provided in Appendix B.

3.1. Radiological and Clinical Evaluations

Overall, excellent radiological and clinical results were observed at the POST stage, i.e., six months after surgery. Specifically, in the 25 patients, the mean hip–knee–ankle angle increased by 6.7° ± 2.3° (from 189.3° ± 3.2° at PRE to 182.6° ± 2.8° at POST), with the discrepancy between PLA and POST equal to 2.1° ± 2.0°. The total KOOS score showed a highly significant improvement ($p < 0.001$) from 56.3 ± 14.0 at PRE stage to 82.1 ± 10.7 at POST stage. Mean VAS pain score decreased highly significantly ($p < 0.001$) from 6.3 ± 1.7 at PRE stage to 1.5 ± 1.7 at POST stage.

3.2. DMA Variables

The number of mesh points contained in the STL files for the three stages were (given as median values and mean ± standard deviation, respectively) 123,542 and 105,081.9 ± 45,068.8

for PRE tibia, 125,680 and 108,409.8 ± 45,982.0 for POST tibia, 9617 and 11,888.1 ± 6007.7 for PLA tibia, 24,502 and 24,375.3 ± 922.0 for PLA fixation plate and 19,280, and 17,494.3 ± 5165.1 for POST fixation plate. In addition, the triangle densities of the surface meshes described in the same STL files (defined as the total number of mesh STL triangles over the total STL area in mm^2) were also calculated. These are also given as median values and mean ± standard deviation, with units triangles/mm^2, respectively, and reported as follows: 10.7 and 9.2 ± 3.7 for PRE tibia, 10.7 and 9.1 ± 3.7 for POST tibia, 0.7 and 0.8 ± 0.3 for PLA tibia, 13.8 and 13.5 ± 0.7 for PLA fixation plate, and 11.2 and 10.1 ± 2.9 for POST fixation plate. Reconstruction of the 3D bone model derived from image segmentation did not result in significant differences between the PRE and POST tibia, both in terms of number of mesh points and triangle density.

Figure 3 provides boxplots showing the values of $\overline{PD}$, $\overline{ND}$, and DSD for all DMA comparisons, while numerical values are given in Table 1. In general, all these values were low, indicating a very high amount of correspondence between the surfaces considered in each comparison.

(i) Overall, a good replication of PLA tibia morphology was achieved in POST (Figures 3 and 4), with average values for $\overline{PD}$ of 1.4 mm and $\overline{ND}$ of −0.9 mm, associated with very small DMA standard deviation (DSD average value 1.6 mm) over the entire patient cohort (Table 1). Most points were in the safe zone (Table 2), although discrepancies were observed, mainly due to the difficulty of excluding the bone allograft (used to fill the osteotomy cut which is the standard practice of the operating surgeon) during image segmentation, thus altering the morphology of the area around the osteotomy in POST with reference to the corresponding one in PLA.

Table 1. DMA outputs (units for all variables mm). $\overline{PD}$ = Positive mean Distance, $\overline{ND}$ = Negative mean Distance, DSD = DMA standard deviation.

DMA Comparison	Variable	Mean	Median	Standard Deviation
(i) POST tibia vs. PLA tibia	$\overline{PD}$	1.4	1.4	0.5
	$\overline{ND}$	−0.9	−0.8	0.4
	DSD	1.6	1.4	0.5
(ii) POST plate vs. PLA plate	$\overline{PD}$	0.4	0.4	0.1
	$\overline{ND}$	−0.2	−0.2	0.1
	DSD	0.4	0.4	0.1
(iii-a) PLA plate vs. PLA tibia	$\overline{PD}$	1.3	1.3	0.2
	$\overline{ND}$	0	0	0
	DSD	0.5	0.4	0.2
(iii-b) POST plate vs. POST tibia	$\overline{PD}$	0.7	0.6	0.4
	$\overline{ND}$	−0.3	−0.3	0.2
	DSD	0.6	0.5	0.2
(iv) POST tib plateau vs. PRE tib plateau	$\overline{PD}$	0.4	0.4	0.2
	$\overline{ND}$	−0.3	−0.2	0.1
	DSD	0.6	0.6	0.2

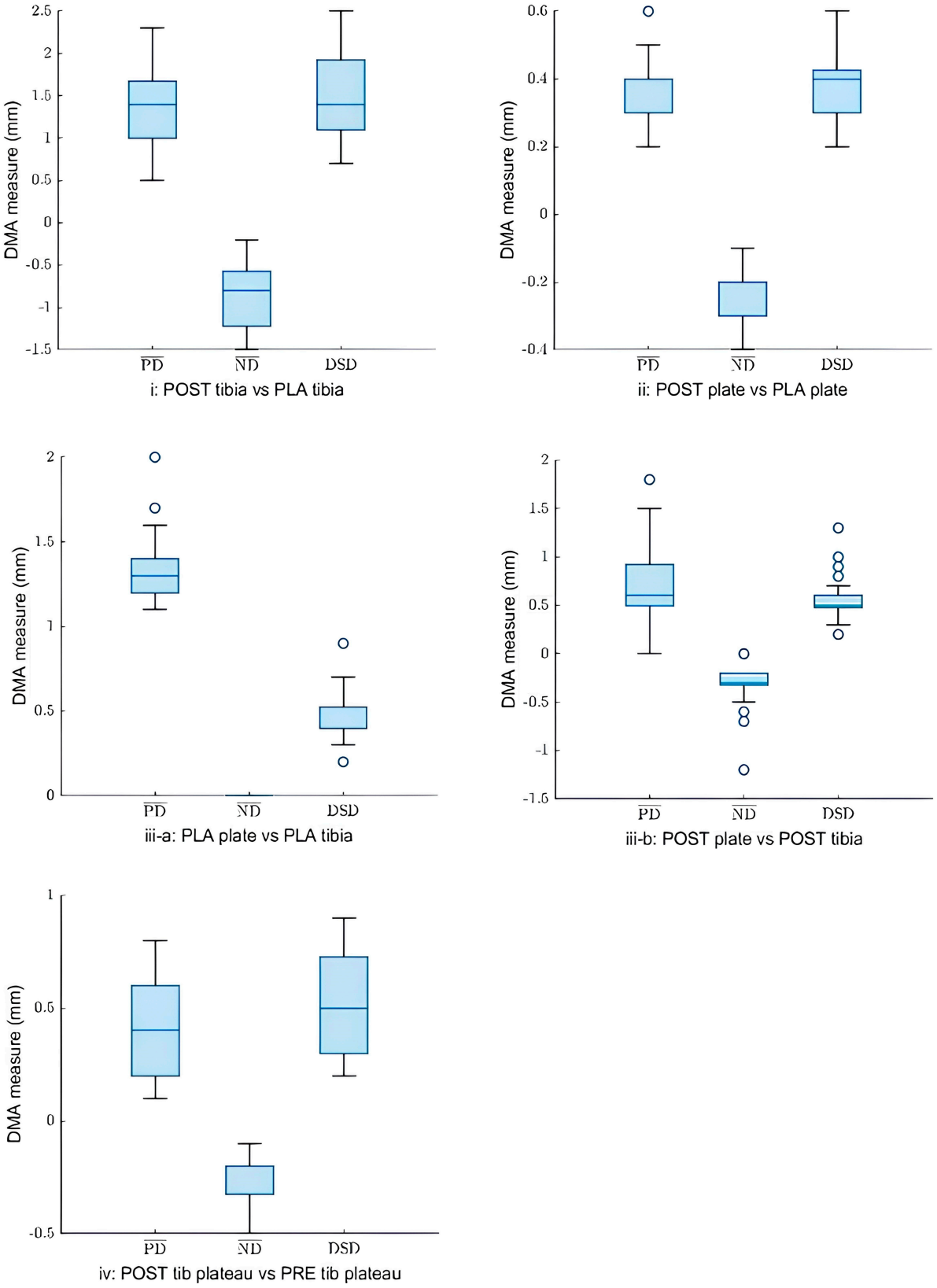

Figure 3. Boxplots for positive mean distance ($\overline{PD}$), negative mean distance ($\overline{ND}$), and DMA standard deviation (DSD) for all sets of surface comparisons.

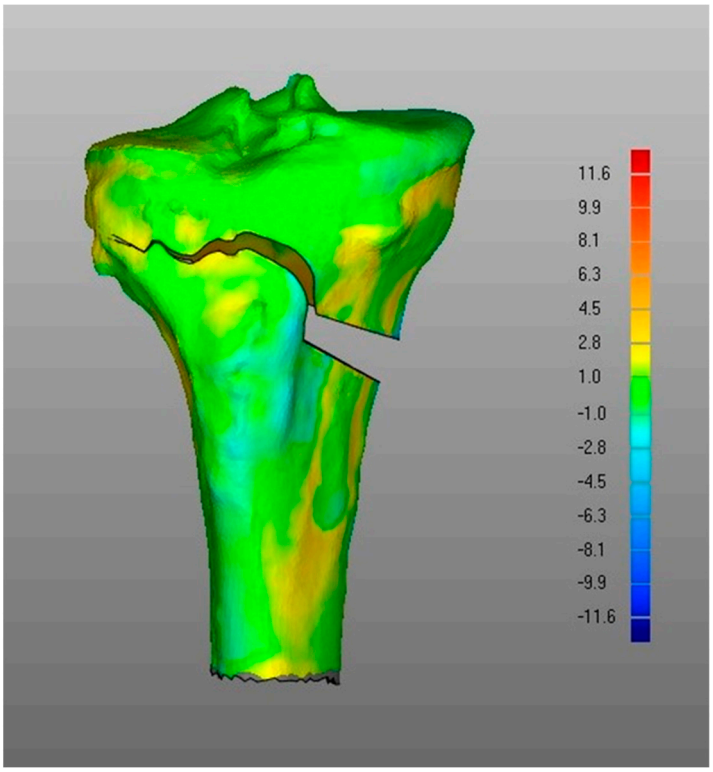

Figure 4. Screenshot of DMA software depicting (i) POST tibia versus PLA tibia. Data from a representative case, the colour scale gives surface deviation in millimetres.

Table 2. % of points with DMA values within three intervals (Δ, in mm). Data are reported in terms of mean, median, and standard deviation.

	DMA Comparison	DMA Range (Δ)	Mean	Median	Standard Deviation
(i)	POST tibia	$\Delta > 1$	31.4	31.8	0.1
	vs.	$\Delta < -1$	10.5	11.2	0.1
	PLA tibia	$-1 \leq \Delta \leq 1$	60.0	59.0	0.1
(ii)	POST fixation plate	$\Delta > 1$	20.5	20.1	0.1
	vs.	$\Delta < -1$	2.5	1.9	0.0
	PLA fixation plate	$-1 \leq \Delta \leq 1$	77	76.8	0.1
(iii-a)	PLA fixation plate	$\Delta > 1$	83.4	83.6	0.1
	vs.	$\Delta < -1$	0	0	0
	PLA tibia	$-1 \leq \Delta \leq 1$	16.6	16.4	0.1
(iii-b)	POST fixation plate	$\Delta > 1$	13.6	6.7	0.2
	vs.	$\Delta < -1$	2.3	1.0	0.0
	POST tibia	$-1 \leq \Delta \leq 1$	84.1	90.4	0.2
(iv)	POST tibial plateau	$\Delta > 1$	13.8	12.5	0.1
	vs.	$\Delta < -1$	4.8	3.4	0.0
	PRE tibial plateau	$-1 \leq \Delta \leq 1$	81.4	85.9	0.1

(ii) The DMA values associated with the deformation of the fixation plate (average for $\overline{PD}$ was 0.4 mm, $\overline{ND}$ was −0.2 mm, with DSD of 0.4 mm) were all less than the critical value, i.e., 1 mm (Table 1) and with most of the points in the safety zone (Table 2),

indicating that the overall shape of the metal plate was maintained after surgery at follow-up (Figures 3 and 5).

(iii) Regarding the matching of the plate surface contour to the tibia, the comparison between PLA, i.e., iii-a (Figure 6 left), and POST, i.e., iii-b (Figure 6 right), the low DMA values (Figure 3 and Table 1) reveal a very good replication of the planned contour matching of the plate to the tibia in the POST condition. In iii-a comparison, there was no negative value, i.e., penetration, of the test surface relative to the reference (Table 2).

(iv) No differences in tibial plateau morphology were found between the PRE and POST stages (Figures 3 and 7, Tables 1 and 2), as the relative DMA values revealing possible changes between surfaces in these two periods were small.

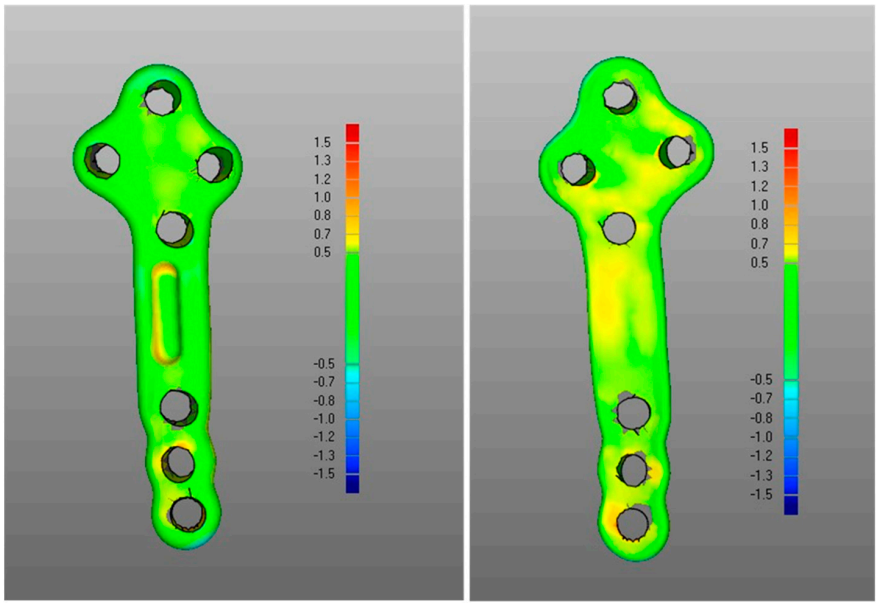

Figure 5. Screenshot (left image front view, right image back view) from DMA software depicting (ii) POST fixation plate versus PLA fixation plate. Data from the representative case above and the colour scale gives surface deviation in millimetres.

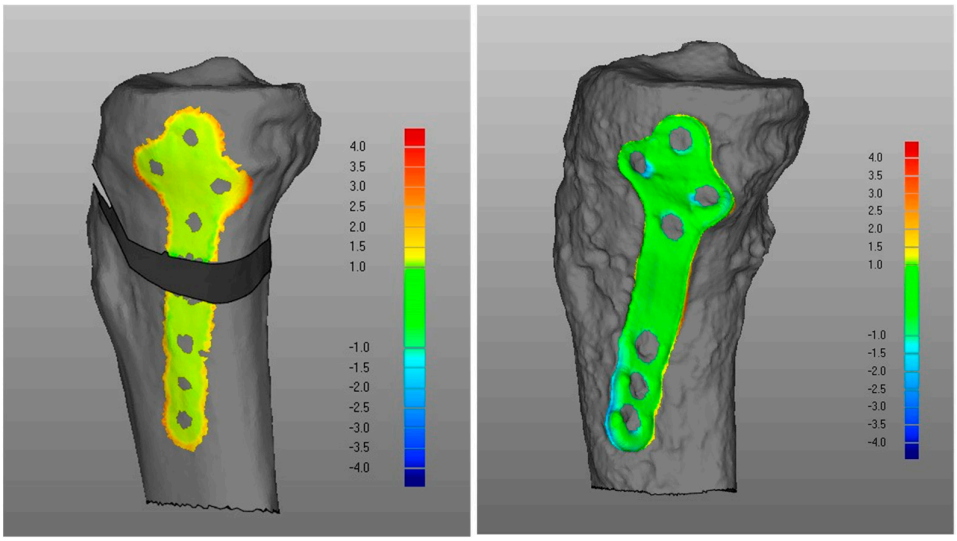

Figure 6. Screenshot of DMA software depicting (iii-a) PLA fixation plate versus PLA tibia (**left**) and (iii-b) POST fixation plate versus POST tibia (**right**). Data from the representative case above and the colour scale gives surface deviation in millimetres.

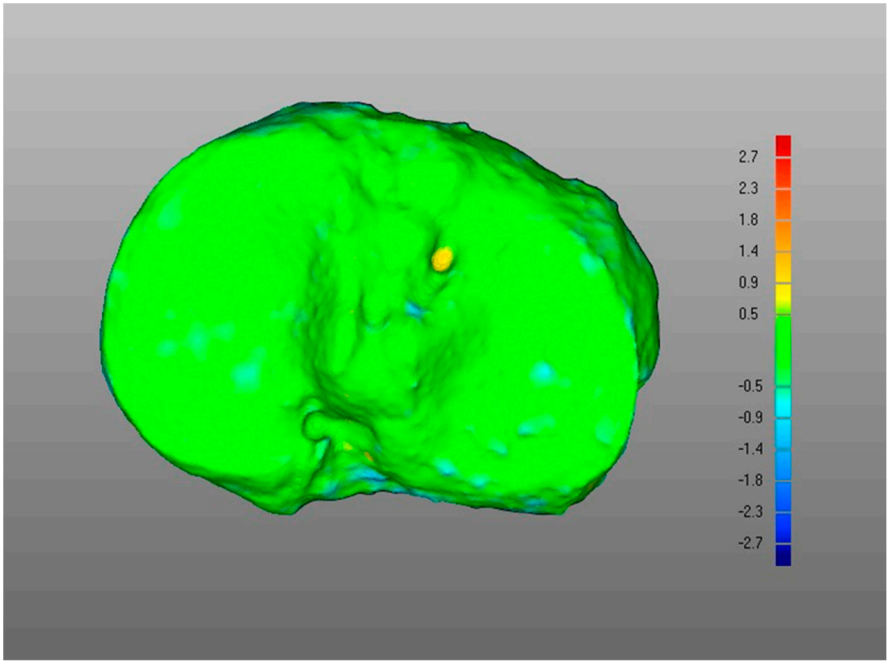

Figure 7. Screenshot of DMA software depicting (iv) POST tibial plateau versus PRE tibial plateau. Data from the representative case above and the colour scale gives surface deviation in millimetres.

4. Discussion

High tibial osteotomy is a highly effective treatment for early-stage knee osteoarthritis [49]; however, it requires appropriate correction and also orthopaedic surgeons must be willing to offer the treatment. It is important to highlight that HTO and unicompartmental knee replacement (UKR) have similar outcomes [50], but HTO is joint preserving, thus offering more future options for treatment. The clinical concern about the difficulty in achieving the planned correction is well articulated by Van den Bempt et al. [28], who state "The accuracy of coronal alignment corrections using conventional HTO falls short". The current study's main purpose was to determine how well a new personalised HTO system actually replicated the planned surgery, going beyond the global commonly used clinical measure of the hip–knee–ankle (HKA) angle. We were able to perform a unique set of measurements in a cohort who had both preoperative and postoperative CT scans. For the first time, a direct 3D comparison between planned and achieved HTO surgery was undertaken. Our findings demonstrate that personalised HTO performed with this system does actually replicate the planned surgery, with the achieved correction matching the planned 3D procedure very well. Overall, the planned osteotomy and fixation plate position was achieved with a discrepancy of considerably less than 2 millimetres (the largest value for the average Positive mean Distance was 1.4 $\pm$ 0.5 mm, Table 1). The current study provides evidence that the planned correction can be achieved with the personalised HTO system used here, and this should provide orthopaedic surgeons the confidence in offering HTO to patients with early knee OA. The results from the distance map analyses are consistent with the changes in the clinical measurements of knee alignment using the hip–knee–ankle angle.

As far as we are aware, there are no other studies which have used this methodology to examine the accuracy of surgically achieving the planned placement of osteotomy bone cuts and stabilisation plates. Thus, it is not possible to compare the findings of the current study with that of other work. A previous cadaver study has shown that the TOKA Personalised HTO procedure achieves a high level of fidelity to the planned correction in terms of changes to HKA [36], which supports the findings of the current study. Patient-specific cutting guides as a means of increasing the accuracy of HTO surgery have been investigated. Munier et al., in a small number of patients, demonstrated that patient-specific

cutting guides allowed HKA correction with two degrees [51]. Fayard et al. reported that personalised cutting guides increase the probability of achieving an accuracy of $\pm 2^{\circ}$ in HKA correction compared to the standard HTO technique [52].

There are some limitations that need to be discussed and some of these are related to the way the 3D surfaces used in the DMA methodology were derived. The PRE and POST geometries were obtained by segmenting CT data, and thus there will be a difference between the PRE dataset and the POST dataset, although these were not significant in terms of the tibial bone models in the present study. The introduction of a metallic implant creates streaking artefacts in CT scans; however, the use of metal artefact reduction processing, such as the one used here, can reduce this considerably [53]. This artefact will give rise to noise in the reconstructed surfaces, as can be seen in our results when using POST data for comparisons. The PLA plate surfaces were generated from Computer-Aided Design (CAD) processes, which have considerably less noise than those from CT data; a very clear reduction in DMA standard deviation is seen for this situation in Figure 3(iii-a). The patient cohort was relatively small, however, for this type of study n = 25 represents a reasonable size.

In distance map analysis, the mean positive and negative distances between the reference and test surfaces are conventionally used to indicate the level of correspondence between reference and test surfaces; however, it is always important to inspect the visualisation of the superposition of the reference and test surfaces. The maximum (or minimum) values can be highly influenced by very localised differences between the surfaces. Figure 5, showing the DMA findings comparing the POST plate position to the PLA plate position, is useful in illustrating this. The POST surface is generated from a reconstruction of a CT scan, whilst the PLA surface is from the CAD representation of the plate. There is a general level of reasonable fit between the two surfaces shown by the large areas of green/yellow. The CT scan reconstruction of some of the small features of the plate will have lower fidelity, particularly in areas of high curvature such as the screw holes and the dished central part of the plate; these may also be more affected by the metal artefact reduction. These regions are highlighted by the localised areas of red indicating distances between the surfaces more than 1.5 mm. Using the maximum (or minimum) difference values between reference and test surfaces will emphasise the effects of local surface deviations, which may not be representative of the majority of the surfaces.

We have included additional examples of the DMA output in the Appendices A and B to show some of the variability in the dataset. As mentioned in Materials and Methods, generating a high-quality surface for planning may result in the segmentation software applying smoothing to the bone surface, which may increase surface differences measured by DMA.

Given the societal and personal impact of knee OA, together with the increase in prevalence, it is becoming increasingly important to be able to offer patients effective treatment at early stages of the disease. Before the large-scale adoption of knee replacement, HTO was a very common treatment for knee OA. Knee replacement surgery has benefitted from decades of improvements in surgical instrumentation that has given surgeons confidence in performing the surgery, whilst HTO has remained relatively unchanged. Personalised HTO simplifies the procedure [31], overcoming the perception of challenging surgery. We have now shown that personalised HTO also is able to achieve the planned correction with a high degree of accuracy. We believe it is important to build surgical confidence in joint-preserving options for treating early knee osteoarthritis. These treatments can be offered at an earlier stage in the disease process, offering patients relief from symptoms and a return to activity possibly decades before a joint replacement will be suitable. Obesity is associated with earlier onset of symptoms, leading many patients to seek joint replacement at a relatively young age thus increasing the risk of early failure. The increase in obesity further emphasises the requirement for effective joint-preserving treatments.

5. Conclusions

Distance map analysis is a useful technique to investigate the accuracy of joint realignment surgery. By comparing 3D models reconstructed from CT scans taken post surgery with models generated from digital planning, we have shown that personalised digitally planned high tibial osteotomy utilising personalised 3D-printed surgical guides and plates enables planned correction and plate placement with an error of less than 2 mm. This work provides evidence to build surgical confidence in being able to offer high tibial osteotomy and making joint-preserving surgery more widely available.

Author Contributions: A.V.: Data Curation, Formal Analysis, Investigation, Writing—Review and Editing. H.S.G.: Conceptualization, Formal Analysis, Investigation, Methodology, Validation, Writing—Review and Editing. S.Z.: Funding Acquisition, Resources, Writing—Review and Editing. A.L.: Conceptualization, Formal Analysis, Funding Acquisition, Project Administration, Resources, Validation, Writing—Original Draft, Writing—Review and Editing. M.O.: Data Curation, Formal Analysis, Investigation, Writing—Review and Editing. F.N.: Data Curation, Investigation, Writing—Review and Editing. A.M.: Software, Visualization, Validation, Writing—Review and Editing. G.D.F.: Data Curation, Formal Analysis, Investigation, Writing—Review and Editing. G.C.: Data Curation, Investigation, Writing—Review and Editing. A.G.: Investigation, Writing—Review and Editing. C.B.: Conceptualization, Formal Analysis, Investigation, Methodology, Project Administration, Supervision, Validation, Writing—Original Draft, Writing—Review and Editing. All authors have read and agreed to the published version of the manuscript.

Funding: This study was partially funded by the Italian Ministry of Health under the "5 per mille" program. Funding for MacLeod was from Versus Arthritis, grant number 22262.

Institutional Review Board Statement: This study was approved by the Ethics Committee (Prot. Gen. 0013355 on 30 October 2019) of the IRCCS Istituto Ortopedico, Bologna-Italy (Cod. CE AVEC: 623/2019/Disp/IOR) and the clinical trial was registered at ClinicalTrials.gov (Cod.: NCT04574570).

Informed Consent Statement: Signed informed consent for participation in this study and to publish related anonymised information/images was obtained by all patients. All patients were above the age of 18 years.

Data Availability Statement: The datasets used and/or analysed during the current study are available from the corresponding author on reasonable request.

Conflicts of Interest: Gill and MacLeod are named inventors on the personalised device patent. All other authors declare that there are no personal or commercial relationships related to this work that would lead to any conflicts of interest.

Appendix A

DMA generates, in addition to the mean values, the Positive Maximum Distance (PMD) and the Negative Maximum Distance (NMD), which are given in Table A1, together with the previous reported mean and standard deviation measures.

Table A1. DMA outputs.

	DMA Comparisons	Parameter	Mean	Median	Standard Deviation
(i)	POST tibia vs. PLA tibia	PMD	7.4	7.2	2.3
		NMD	−5.4	−5.2	1.4
		$\overline{PD}$	1.4	1.4	0.5
		$\overline{ND}$	−0.9	−0.8	0.4
		DSD	1.6	1.4	0.5

Table A1. *Cont.*

	DMA Comparisons	Parameter	Mean	Median	Standard Deviation
(ii)	POST fixation plate vs. PLA fixation plate	PMD	2.3	1.9	1.2
		NMD	−1.9	−1.8	0.5
		$\overline{PD}$	0.4	0.4	0.1
		$\overline{ND}$	−0.2	−0.2	0.1
		DSD	0.4	0.4	0.1
(iii-a)	PLA fixation plate vs. PLA tibia	PMD	5.0	4.8	1.2
		NMD	0.0	0.0	0.0
		$\overline{PD}$	1.3	1.3	0.2
		$\overline{ND}$	0.0	0.0	0.0
		DSD	0.5	0.4	0.2
(iii-b)	POST fixation plate vs. POST tibia	PMD	3.2	3.3	1.2
		NMD	−1.6	−1.4	1.1
		$\overline{PD}$	0.7	0.6	0.4
		$\overline{ND}$	−0.3	−0.3	0.2
		DSD	0.6	0.5	0.2
(iv)	POST tibial plateau vs. PRE tibial plateau	PMD	3.8	3.2	1.8
		NMD	−2.3	−2.0	1.3
		$\overline{PD}$	0.4	0.4	0.2
		$\overline{ND}$	−0.3	−0.2	0.1
		DSD	0.6	0.6	0.2

Appendix B

Distance map analysis was performed for all patients in the cohort. Figures A1–A4 below are the DMA software screenshots of an alternative patient case to the one shown in Figures 4–7.

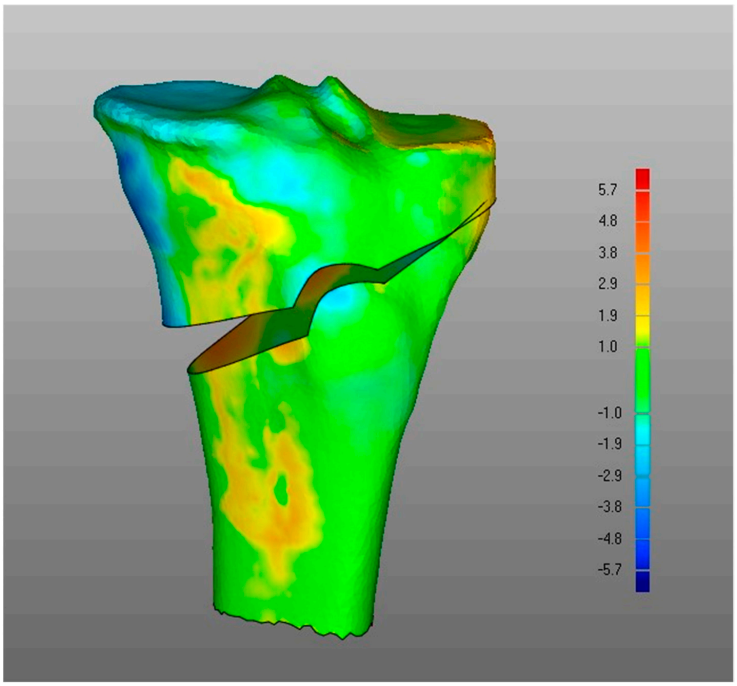

Figure A1. Screenshot of DMA software depicting (i) POST tibia versus PLA tibia. Data from an alternative case to the one shown in Figure 4. The colour scale gives surface deviation in millimetres.

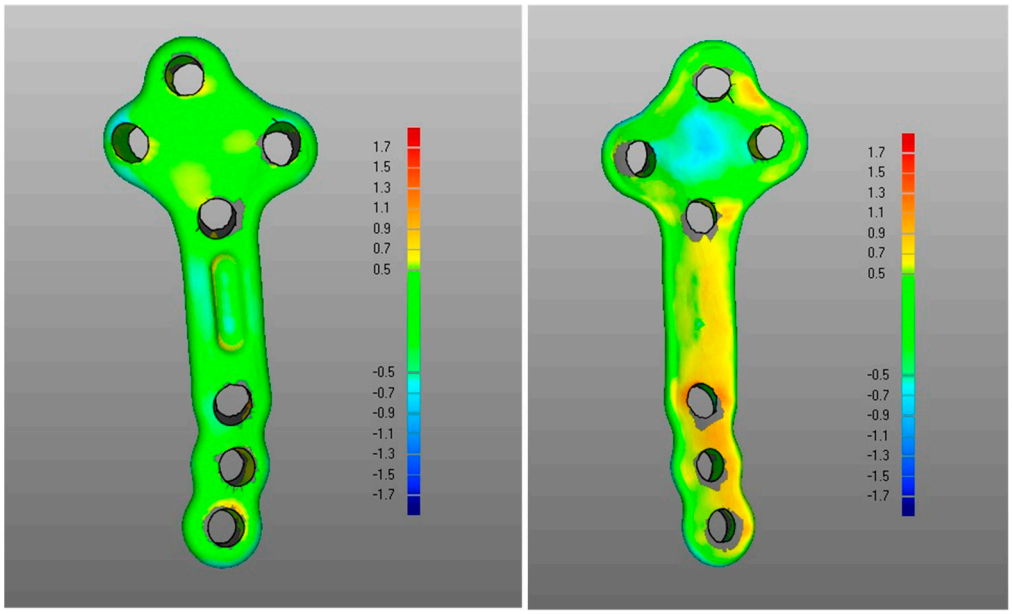

Figure A2. Screenshot (left image front view, right image back view) from DMA software depicting (ii) POST fixation plate versus PLA fixation plate. Data from an alternative case to the one shown in Figure 5. The colour scale gives surface deviation in millimetres.

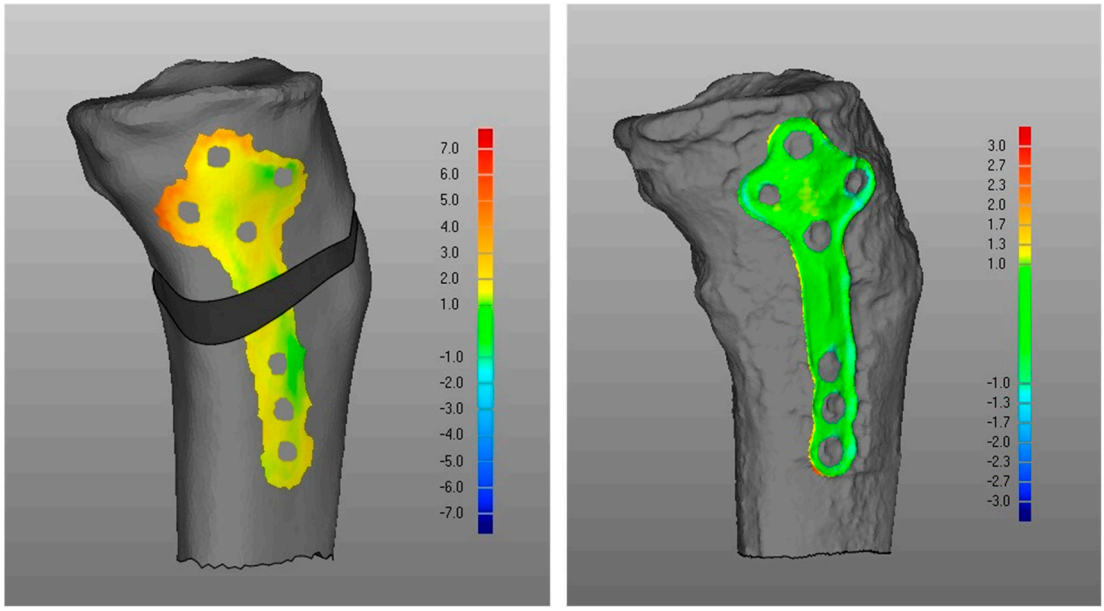

Figure A3. Screenshot of DMA software depicting (iii-a) PLA fixation plate versus PLA tibia (**left**) and (iii-b) POST fixation plate versus POST tibia (**right**). Data from an alternative case to the one shown in Figure 6. The colour scale gives surface deviation in millimetres.

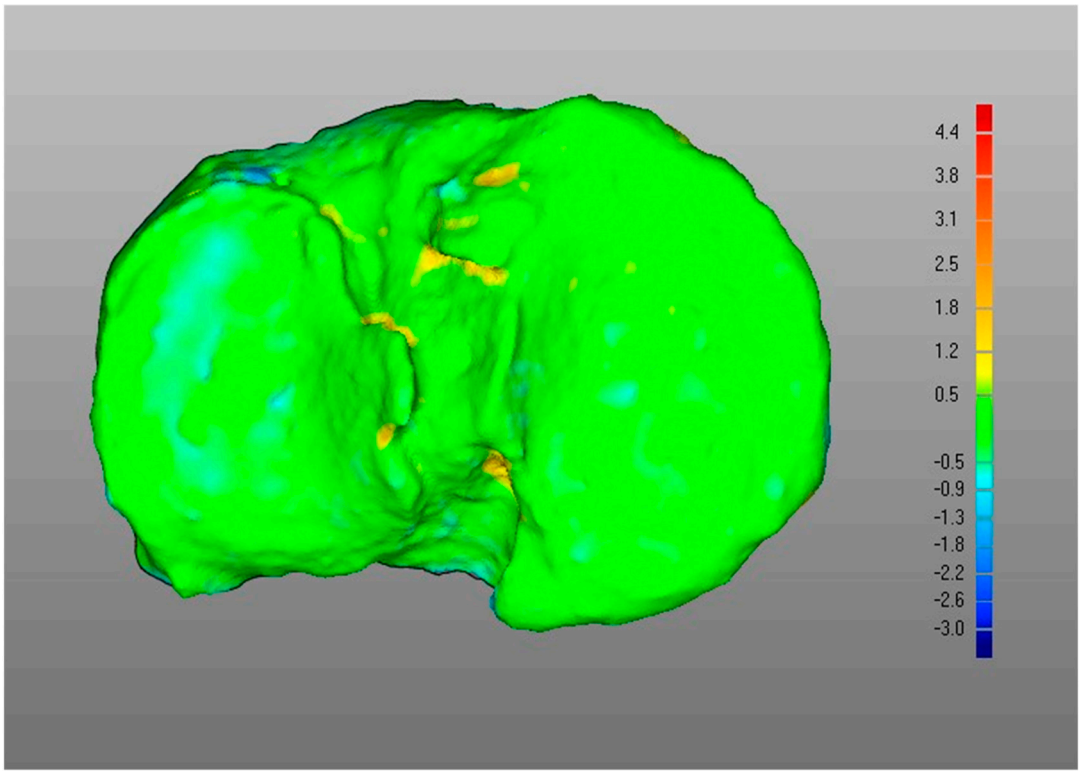

Figure A4. Screenshot of DMA software depicting (iv) POST tibial plateau versus PRE tibial plateau. Data from an alternative case to the one shown in Figure 7. The colour scale gives surface deviation in millimetres.

References

1. Peat, G.; McCarney, R.; Croft, P. Knee pain and osteoarthritis in older adults: A review of community burden and current use of primary health care. *Ann. Rheum. Dis.* **2001**, *60*, 91–97. [CrossRef] [PubMed]
2. Hermans, J.; Koopmanschap, M.A.; Bierma-Zeinstra, S.M.; van Linge, J.H.; Verhaar, J.A.; Reijman, M.; Burdorf, A. Productivity costs and medical costs among working patients with knee osteoarthritis. *Arthritis Care Res.* **2012**, *64*, 853–861. [CrossRef] [PubMed]
3. Xie, F.; Kovic, B.; Jin, X.; He, X.; Wang, M.; Silvestre, C. Economic and Humanistic Burden of Osteoarthritis: A Systematic Review of Large Sample Studies. *Pharmacoeconomics* **2016**, *34*, 1087–1100. [CrossRef] [PubMed]
4. Cui, A.; Li, H.; Wang, D.; Zhong, J.; Chen, Y.; Lu, H. Global, regional prevalence, incidence and risk factors of knee osteoarthritis in population-based studies. *EClinicalMedicine* **2020**, *29–30*, 100587. [CrossRef]
5. Prieto-Alhambra, D.; Judge, A.; Javaid, M.K.; Cooper, C.; Diez-Perez, A.; Arden, N.K. Incidence and risk factors for clinically diagnosed knee, hip and hand osteoarthritis: Influences of age, gender and osteoarthritis affecting other joints. *Ann. Rheum. Dis.* **2014**, *73*, 1659–1664. [CrossRef] [PubMed]
6. Nguyen, U.S.; Zhang, Y.; Zhu, Y.; Niu, J.; Zhang, B.; Felson, D.T. Increasing prevalence of knee pain and symptomatic knee osteoarthritis: Survey and cohort data. *Ann. Intern. Med.* **2011**, *155*, 725–732. [CrossRef] [PubMed]
7. Turkiewicz, A.; Petersson, I.F.; Bjork, J.; Hawker, G.; Dahlberg, L.E.; Lohmander, L.S.; Englund, M. Current and future impact of osteoarthritis on health care: A population-based study with projections to year 2032. *Osteoarthr. Cartil.* **2014**, *22*, 1826–1832. [CrossRef] [PubMed]
8. Perruccio, A.V.; Power, J.D.; Badley, E.M. Revisiting arthritis prevalence projections—It's more than just the aging of the population. *J. Rheumatol.* **2006**, *33*, 1856–1862. [PubMed]
9. Wallace, I.J.; Worthington, S.; Felson, D.T.; Jurmain, R.D.; Wren, K.T.; Maijanen, H.; Woods, R.J.; Lieberman, D.E. Knee osteoarthritis has doubled in prevalence since the mid-20th century. *Proc. Natl. Acad. Sci. USA* **2017**, *114*, 9332–9336. [CrossRef] [PubMed]
10. Swain, S.; Coupland, C.; Strauss, V.; Mallen, C.; Kuo, C.F.; Sarmanova, A.; Bierma-Zeinstra, S.M.A.; Englund, M.; Prieto-Alhambra, D.; Doherty, M.; et al. Clustering of comorbidities and associated outcomes in people with osteoarthritis—A UK Clinical Practice Research Datalink study. *Osteoarthr. Cartil.* **2022**, *30*, 702–713. [CrossRef] [PubMed]
11. Cleveland, R.J.; Alvarez, C.; Schwartz, T.A.; Losina, E.; Renner, J.B.; Jordan, J.M.; Callahan, L.F. The impact of painful knee osteoarthritis on mortality: A community-based cohort study with over 24 years of follow-up. *Osteoarthr. Cartil.* **2019**, *27*, 593–602. [CrossRef] [PubMed]

12. Patel, A.; Pavlou, G.; Mujica-Mota, R.E.; Toms, A.D. The epidemiology of revision total knee and hip arthroplasty in England and Wales: A comparative analysis with projections for the United States. A study using the National Joint Registry dataset. *Bone Joint J.* **2015**, *97-B*, 1076–1081. [CrossRef] [PubMed]
13. Kurtz, S.; Ong, K.; Lau, E.; Mowat, F.; Halpern, M. Projections of primary and revision hip and knee arthroplasty in the United States from 2005 to 2030. *J. Bone Joint Surg. Am.* **2007**, *89*, 780–785. [CrossRef] [PubMed]
14. National Institute for Health and Care Excellence (NICE). *Evidence Review for Total Knee Replacement: Guideline (NICE Guideline, No. 157)*; National Guideline Centre: London, UK, 2020.
15. London, N.J.; Miller, L.E.; Block, J.E. Clinical and economic consequences of the treatment gap in knee osteoarthritis management. *Med. Hypotheses* **2011**, *76*, 887–892. [CrossRef] [PubMed]
16. Silverman, S.; Thakkar, S.; Sell, H.; White, A.G.; Downes, N.; Pajerowski, W.; Robinson, R.L.; Beck, C.G.; Emir, B.; Schepman, P. All-Cause Health Care and Work Loss Burden Associated With Nonsteroidal Anti-Inflammatory Drug and Opioid Treatment in Employed Patients With Osteoarthritis. *J. Occup. Environ. Med.* **2022**, *64*, 699–706. [CrossRef] [PubMed]
17. Silverman, S.; Rice, J.B.; White, A.G.; Beck, C.G.; Robinson, R.L.; Fernan, C.; Schepman, P. Clinical and economic burden of prescribing tramadol and other opioids for patients with osteoarthritis in a commercially insured population in the United States. *Pain* **2022**, *163*, 75–82. [CrossRef] [PubMed]
18. Yu, D.; Hellberg, C.; Appleyard, T.; Dell'Isola, A.; Thomas, G.E.R.; Turkiewicz, A.; Englund, M.; Peat, G. Opioid use prior to total knee replacement: Comparative analysis of trends in England and Sweden. *Osteoarthr. Cartil.* **2022**, *30*, 815–822. [CrossRef] [PubMed]
19. Ledingham, J.; Regan, M.; Jones, A.; Doherty, M. Radiographic patterns and associations of osteoarthritis of the knee in patients referred to hospital. *Ann. Rheum. Dis.* **1993**, *52*, 520–526. [CrossRef] [PubMed]
20. Zuiderbaan, H.A.; van der List, J.P.; Kleeblad, L.J.; Appelboom, P.; Kort, N.P.; Pearle, A.D.; Rademakers, M.V. Modern Indications, Results, and Global Trends in the Use of Unicompartmental Knee Arthroplasty and High Tibial Osteotomy in the Treatment of Isolated Medial Compartment Osteoarthritis. *Am. J. Orthop.* **2016**, *45*, E355–E361. [PubMed]
21. Santoso, M.B.; Wu, L. Unicompartmental knee arthroplasty, is it superior to high tibial osteotomy in treating unicompartmental osteoarthritis? A meta-analysis and systemic review. *J. Orthop. Surg. Res.* **2017**, *12*, 50. [CrossRef]
22. Spahn, G.; Hofmann, G.O.; von Engelhardt, L.V.; Li, M.; Neubauer, H.; Klinger, H.M. The impact of a high tibial valgus osteotomy and unicondylar medial arthroplasty on the treatment for knee osteoarthritis: A meta-analysis. *Knee Surg. Sports Traumatol. Arthrosc.* **2013**, *21*, 96–112. [CrossRef] [PubMed]
23. Cao, Z.; Mai, X.; Wang, J.; Feng, E.; Huang, Y. Unicompartmental Knee Arthroplasty vs High Tibial Osteotomy for Knee Osteoarthritis: A Systematic Review and Meta-Analysis. *J. Arthroplast.* **2018**, *33*, 952–959. [CrossRef] [PubMed]
24. Hunt, L.P.; Blom, A.W.; Matharu, G.S.; Kunutsor, S.K.; Beswick, A.D.; Wilkinson, J.M.; Whitehouse, M.R. Patients Receiving a Primary Unicompartmental Knee Replacement Have a Higher Risk of Revision but a Lower Risk of Mortality Than Predicted Had They Received a Total Knee Replacement: Data From the National Joint Registry for England, Wales, Northern Ireland, and the Isle of Man. *J. Arthroplast.* **2021**, *36*, 471–477. [CrossRef]
25. Hansen, E.N.; Ong, K.L.; Lau, E.; Kurtz, S.M.; Lonner, J.H. Unicondylar Knee Arthroplasty Has Fewer Complications but Higher Revision Rates Than Total Knee Arthroplasty in a Study of Large United States Databases. *J. Arthroplast.* **2019**, *34*, 1617–1625. [CrossRef] [PubMed]
26. Di Martino, A.; Bordini, B.; Barile, F.; Ancarani, C.; Digennaro, V.; Faldini, C. Unicompartmental knee arthroplasty has higher revisions than total knee arthroplasty at long term follow-up: A registry study on 6453 prostheses. *Knee Surg. Sports Traumatol. Arthrosc.* **2021**, *29*, 3323–3329. [CrossRef] [PubMed]
27. Ben-Shlomo, Y.; Blom, A.; Boulton, C.; Brittain, R.; Clark, E.; Dawson-Bowling, S.; Deere, K.; Esler, C.; Espinoza, O.; Goldberg, A.; et al. *The National Joint Registry 18th Annual Report 2021*; National Joint Registry: London, UK, 2021. [PubMed]
28. Van den Bempt, M.; Van Genechten, W.; Claes, T.; Claes, S. How accurately does high tibial osteotomy correct the mechanical axis of an arthritic varus knee? A systematic review. *Knee* **2016**, *23*, 925–935. [CrossRef] [PubMed]
29. Hsu, R.W.; Himeno, S.; Coventry, M.B.; Chao, E.Y. Normal axial alignment of the lower extremity and load-bearing distribution at the knee. *Clin. Orthop. Relat. Res.* **1990**, *255*, 215–227. [CrossRef]
30. Spahn, G. Complications in high tibial (medial opening wedge) osteotomy. *Arch. Orthop. Trauma. Surg.* **2004**, *124*, 649–653. [CrossRef] [PubMed]
31. Zaffagnini, S.; Dal Fabbro, G.; Belvedere, C.; Leardini, A.; Caravelli, S.; Lucidi, G.A.; Agostinone, P.; Mosca, M.; Neri, M.P.; Grassi, A. Custom-Made Devices Represent a Promising Tool to Increase Correction Accuracy of High Tibial Osteotomy: A Systematic Review of the Literature and Presentation of Pilot Cases with a New 3D-Printed System. *J. Clin. Med.* **2022**, *11*, 5717. [CrossRef]
32. Belvedere, C.; Macleod, A.; Leardini, A.; Grassi, A.; Fabbro, G.D.; Zaffagnini, S.; Gill, H.S. 3D Medical Imaging Analysis, Patient-Specific Instrumentation and Individualized Implant Design, with Additive Manufacturing Creates a New Personalized High Tibial Osteotomy Treatment Option. *J. Mech. Med. Biol.* **2023**, *23*, 2340041. [CrossRef]
33. MacLeod, A.R.; Peckham, N.; Serrancoli, G.; Rombach, I.; Hourigan, P.; Mandalia, V.I.; Toms, A.D.; Fregly, B.J.; Gill, H.S. Personalised high tibial osteotomy has mechanical safety equivalent to generic device in a case-control in silico clinical trial. *Commun. Med.* **2021**, *1*, 6. [CrossRef] [PubMed]

34. Belvedere, C.; Gill, H.S.; Ortolani, M.; Sileoni, N.; Zaffagnini, S.; Norvillo, F.; MacLeod, A.; Dal Fabbro, G.; Grassi, A.; Leardini, A. Instrumental gait analysis and tibial plateau modelling to support pre- and post-operative evaluations in personalized high tibial osteotomy. *Appl. Sci.* **2023**, *13*, 12425. [CrossRef]
35. Jeong, S.H.; Samuel, L.T.; Acuna, A.J.; Kamath, A.F. Patient-specific high tibial osteotomy for varus malalignment: 3D-printed plating technique and review of the literature. *Eur. J. Orthop. Surg. Traumatol.* **2022**, *32*, 845–855. [CrossRef] [PubMed]
36. MacLeod, A.R.; Mandalia, V.I.; Mathews, J.A.; Toms, A.D.; Gill, H.S. Personalised 3D Printed high tibial osteotomy achieves a high level of accuracy: 'IDEAL' preclinical stage evaluation of a novel patient specific system. *Med. Eng. Phys.* **2022**, *108*, 103875. [CrossRef] [PubMed]
37. Zaffagnini, S.; Dal Fabbro, G.; Lucidi, G.A.; Agostinone, P.; Belvedere, C.; Leardini, A.; Grassi, A. Personalised opening wedge high tibial osteotomy with patient-specific plates and instrumentation accurately controls coronal correction and posterior slope: Results from a prospective first case series. *Knee* **2023**, *44*, 89–99. [CrossRef] [PubMed]
38. Durastanti, G.; Leardini, A.; Siegler, S.; Durante, S.; Bazzocchi, A.; Belvedere, C. Comparison of cartilage and bone morphological models of the ankle joint derived from different medical imaging technologies. *Quant. Imaging Med. Surg.* **2019**, *9*, 1368–1382. [CrossRef] [PubMed]
39. Honigmann, P.; Keller, M.; Devaux-Voumard, N.; Thieringer, F.M.; Sutter, D. Distance mapping in three-dimensional virtual surgical planning in hand, wrist and forearm surgery: A tool to avoid mistakes. *Int. J. Comput. Assist. Radiol. Surg.* **2023**, *18*, 565–574. [CrossRef] [PubMed]
40. Negrillo-Cardenas, J.; Jimenez-Perez, J.R.; Canada-Oya, H.; Feito, F.R.; Delgado-Martinez, A.D. Automatic detection of landmarks for the analysis of a reduction of supracondylar fractures of the humerus. *Med. Image Anal.* **2020**, *64*, 101729. [CrossRef]
41. Perez-Cano, F.D.; Jimenez-Perez, J.R.; Molina-Viedma, A.J.; Lopez-Alba, E.; Luque-Luque, A.; Delgado-Martinez, A.; Diaz-Garrido, F.A.; Jimenez-Delgado, J.J. Human femur fracture by mechanical compression: Towards the repeatability of bone fracture acquisition. *Comput. Biol. Med.* **2023**, *164*, 107249. [CrossRef]
42. Ruggeri, M.; Gill, H.S.; Leardini, A.; Zaffagnini, S.; MacLeod, A.; Ortolani, M.; Faccia, F.; Grassi, A.; Fabbro, G.D.; Durante, S.; et al. Superimposition of ground reaction force on tibial-plateau supporting diagnostics and post-operative evaluations in high-tibial osteotomy. A novel methodology. *Gait Posture* **2022**, *94*, 144–152. [CrossRef]
43. Roos, E.M.; Lohmander, L.S. The Knee injury and Osteoarthritis Outcome Score (KOOS): From joint injury to osteoarthritis. *Health Qual. Life Outcomes* **2003**, *1*, 64. [CrossRef] [PubMed]
44. Delgado, D.A.; Lambert, B.S.; Boutris, N.; McCulloch, P.C.; Robbins, A.B.; Moreno, M.R.; Harris, J.D. Validation of Digital Visual Analog Scale Pain Scoring With a Traditional Paper-based Visual Analog Scale in Adults. *J. Am. Acad. Orthop. Surg. Glob. Res. Rev.* **2018**, *2*, e088. [CrossRef] [PubMed]
45. Leardini, A.; Durante, S.; Belvedere, C.; Caravaggi, P.; Carrara, C.; Berti, L.; Lullini, G.; Giacomozzi, C.; Durastanti, G.; Ortolani, M.; et al. Weight-bearing CT Technology in Musculoskeletal Pathologies of the Lower Limbs: Techniques, Initial Applications, and Preliminary Combinations with Gait-Analysis Measurements at the Istituto Ortopedico Rizzoli. *Semin. Musculoskelet. Radiol.* **2019**, *23*, 643–656. [CrossRef] [PubMed]
46. Nardi, C.; Salerno, S.; Molteni, R.; Occhipinti, M.; Grazzini, G.; Norberti, N.; Cordopatri, C.; Colagrande, S. Radiation dose in non-dental cone beam CT applications: A systematic review. *Radiol. Med.* **2018**, *123*, 765–777. [CrossRef] [PubMed]
47. Holbrook, H.S.; Bowers, A.F.; Mahmoud, K.; Kelly, D.M. Weight-Bearing Computed Tomography of the Foot and Ankle in the Pediatric Population. *J. Pediatr. Orthop.* **2022**, *42*, 321–326. [CrossRef] [PubMed]
48. Lemmens, C.; Faul, D.; Nuyts, J. Suppression of metal artifacts in CT using a reconstruction procedure that combines MAP and projection completion. *IEEE Trans. Med. Imaging* **2009**, *28*, 250–260. [CrossRef]
49. Dal Fabbro, G.; Grassi, A.; Agostinone, P.; Lucidi, G.A.; Fajury, R.; Ravindra, A.; Zaffagnini, S. High survivorship rate and good clinical outcomes after high tibial osteotomy in patients with radiological advanced medial knee osteoarthritis: A systematic review. *Arch. Orthop. Trauma. Surg.* **2024**. [CrossRef]
50. Teo, S.J.; Purnomo, G.; Koh, D.T.S.; Soong, J.; Yeo, W.; Razak, H.; Lee, K.H. High tibial osteotomy versus unicompartmental knee arthroplasty in advanced medial compartmental knee arthrosis: A comparative study with propensity score matched analysis. *Knee* **2024**, *49*, 116–124. [CrossRef] [PubMed]
51. Munier, M.; Donnez, M.; Ollivier, M.; Flecher, X.; Chabrand, P.; Argenson, J.N.; Parratte, S. Can three-dimensional patient-specific cutting guides be used to achieve optimal correction for high tibial osteotomy? Pilot study. *Orthop. Traumatol. Surg. Res.* **2017**, *103*, 245–250. [CrossRef]
52. Fayard, J.M.; Saad, M.; Gomes, L.; Kacem, S.; Abid, H.; Vieira, T.D.; Lambrey, P.J.; Ollivier, M.; Thaunat, M. Patient-specific cutting guides increase accuracy of medial opening wedge high tibial osteotomy procedure: A retrospective case-control study. *J. Exp. Orthop.* **2024**, *11*, e12013. [CrossRef]
53. Kuzu, T.E.; Kis, H.C. Effect of different cone beam computed tomography settings on artifact production in titanium and zirconia dental implants: An in vitro study. *Dent. Med. Probl.* **2024**, *61*, 233–239. [CrossRef] [PubMed]